

Design and simulation of a poly(vinyl alcohol)–bacterial cellulose nanocomposite mechanical aortic heart valve prosthesis

H Mohammadi^{1*}, D Boughner^{1,2}, L E Millon¹, and W K Wan^{1,3}

¹Department of Biomedical Engineering, Faculty of Engineering, The University of Western Ontario, London, Ontario, Canada

²London Health Sciences Center, London, Ontario, Canada

³Department of Chemical and Biochemical Engineering, The University of Western Ontario, London, Ontario, Canada

The manuscript was received on 31 July 2008 and was accepted after revision for publication on 21 April 2009.

DOI: 10.1243/09544119JEIM493

Abstract: In this study, a polymeric aortic heart valve made of poly(vinyl alcohol) (PVA)–bacterial cellulose (BC) nanocomposite is simulated and designed using a hyperelastic non-linear anisotropic material model. A novel nanocomposite biomaterial combination of 15 wt % PVA and 0.5 wt % BC is developed in this study. The mechanical properties of the synthesized PVA–BC are similar to those of the porcine heart valve in both the principal directions. To design the geometry of the leaflets an advance surfacing technique is employed. A Galerkin-based non-linear finite element method is applied to analyse the mechanical behaviour of the leaflet in the closing and opening phases under physiological conditions. The model used in this study can be implemented in mechanical models for any soft tissues such as articular cartilage, tendon, and ligament.

Keywords: finite element method, mechanical heart valves, poly(vinyl alcohol), bacterial cellulose, soft tissue, anisotropy, non-linearity

1 INTRODUCTION

Trileaflet polymeric heart valve (HV) prostheses have been considered an effective alternative replacements for failed HVs as they have a similar geometry and structure to those of the native valve. Based on this similarity, they have better haemodynamics with lower pressure gradient, central flow, and larger orifice area compared with the bileaflet mechanical counterparts. The most important features for a polymer to be employed in HV prostheses are biocompatibility, haemocompatibility, and resistance to calcifications, with mechanical properties similar to those of the native HV tissue. The main problems with polymeric HVs are failure due to tearing and calcification of the leaflets under high

dynamic tensile bending stress and oxidative reactions with blood [1]. From a structural and mechanical properties point of view, it has been hypothesized that valve leaflet material fabricated from fibre-reinforced composite material that mimics the native valve leaflet structure and properties will optimize leaflet stresses and decrease tears and perforations [1]. Materials that have been considered over the past years including poly(tetrafluoroethylene), poly(vinyl chloride), segmented poly(urethane), silicon rubber, and poly(ether urethane urea) all have shortcomings in fatigue life and calcification complications [1–4].

Mechanical modelling is an effective tool to analyse and optimize the design of prosthetic HVs. In early studies, isotropic models and later anisotropic and time-dependent models with higher degrees of complexity were considered to simulate the dynamics of HVs and the stress on leaflets in both the closing and the opening phases of the cardiac cycle [5–14]. Li *et al.* [15] and Luo *et al.* [16]

*Corresponding author: Department of Biomedical Engineering, Faculty of Engineering, The University of Western Ontario, London, Ontario N6A 5B9, Canada.
email: hmohamm3@uwo.ca

presented a non-linear anisotropic model for porcine HV and analysed the effect of geometry and non-linearity of the tissue mechanical properties on stress distribution in a porcine HV. De Hart *et al.* [17] studied the effect of collagen fibres on the mechanics and haemodynamics of a trileaflet aortic valve using numerical methods. Recently, Kim *et al.* [18] have provided a new approach using a Fung-type elastic constitutive model for pericardial bio-prosthetic HVs accounting for anisotropy and hyperelasticity of the HV leaflets.

Bacterial cellulose (BC) and poly(vinyl alcohol) (PVA) (a hydrophilic biocompatible polymer) as an anisotropic nanocomposite have valuable characteristics for biomedical applications [19]. Millon and Wan *et al.* [20] reported a material properties match between PVA and porcine aortic root, but this was not the case for the HV leaflets [20]. Guhadós *et al.* [21] measured the elastic modulus of a single bacterial cellulose fibre using atomic force microscopy, indicating that the stiffness of BC fibres was sufficient for reinforcement of PVA sheets.

In this study an anisotropic and non-linear finite element (FE) model is implemented to study the mechanical behaviour of leaflets in a PVA-BC HV prosthesis under physiological conditions. Also, a methodology to design trileaflet aortic HV prostheses is presented.

2 METHOD

2.1 Experimental set-up

PVA, 99+ per cent hydrolysed and with a molecular weight of 146 000–186 000, was used for the solution preparation. A suspension of 0.877 wt% BC in distilled water was used, which was produced in shake flasks by fermentation process using the bacterium *Acetobacter xylinum*, as described by Guhadós *et al.* [21]. Dry PVA and distilled water were added to the BC suspension to obtain a 15 wt% PVA with 0.5 wt% BC mixture. The PVA-BC solution was transferred into three aluminium moulds and placed in a heated-refrigerated circulator (VWR model 1180S), which cycled the moulds once between 20 °C and -20 °C at 0.1 °C/min to give cycle 1 samples, following the same procedure reported by Millon and Wan. [20]. To create the maximum anisotropy in the longitudinal direction, an initial strain of 75 per cent was applied for all three samples, as reported in reference [19]. The cycle 1 samples were transferred and stretched, while placing an extra sample of non-stretched PVA-BC

hydrogel (cycle 1) in the moulds as controls. The moulds were cycled, using the above-mentioned freeze-thaw cycle procedure, and a mould was removed at the end of cycles 2, 4, and 6.

The testing equipment consists of a servohydraulic testing machine (Instron 8872) equipped with a 1 kgf load cell. After measuring the sample thickness, testing was carried out inside a Plexiglas tank filled with distilled water kept at 37 °C. All the specimens were secured on to tissue grips (about 10 mm grip to grip), and tensile tests were performed at a strain rate of 40 mm/s to a maximum of 60 per cent strain. Prior to the tensile tests, all specimens were preconditioned with ten loading and unloading cycles with an amplitude of 5 cm (peak-to-peak valve of 10 cm) and a frequency of 2 cycles/s.

The mechanical properties of biological tissues are strain or loading rate dependent owing to their viscoelastic nature. Biological tissues typically become stiffer with increasing strain rate. As such, predetermined and tightly controlled strain or loading rates must be maintained during testing. Further, many biological tissues in their normal state are preconditioned (e.g. the ligament) while many are not (e.g. the brain). For a tissue that has not been preconditioned, its response to load or displacement from one cycle to the next will not be similar and hence results will not be consistent. Depending on the type of tissue being tested or the response of interest (e.g. sudden impact or fatigue failure), preconditioning as part of the testing protocol may or may not be necessary.

2.2 Constitutive model

This section describes the development of a constitutive model for the modelling of a leaflet structure made from PVA-BC as a soft anisotropic material. The constitutive model describes the necessary mechanical behaviour of the biomaterial used, such as non-linear behaviour, large deformation, anisotropy, and distinct behaviour in tension. This approach is based on the theory of a large strain in continuum mechanics using a strain energy density function in both circumferential and longitudinal directions separately (Fig. 1).

The key idea is to define a stress energy density function from which the stress can be derived by taking the partial derivatives conjugate to the strain. In theory, the selection of such a strain energy density function is unlimited and arbitrary and NASTRAN supports most of the generic strain energy density functions. A choice was made to use a

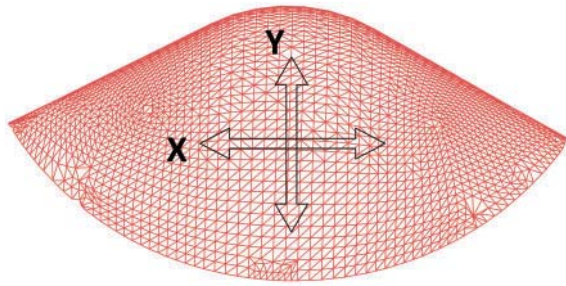


Fig. 1 The circumferential (X) and longitudinal (Y) directions of the anisotropic leaflets of a PVA–BC heart valve viewed from the top

complete second-order polynomial form because it appears that five terms are sufficient for the present application. One advantage of the polynomial material model, in this case, is that it approximates all the testing data nicely. Additionally, for theoretical simplicity, hyperelastic materials are assumed to be incompressible. An incompressible material will cause volumetric locking that requires special treatment on element formulation. This limits the choice of element types for stress analysis on a nearly incompressible hyperelastic material to first-order solid elements, structural elements, and second-order solid elements.

2.3 The Mooney–Rivlin hyperelastic model

This model is defined by a strain energy density function given as a function of principal strains, which are also called strain invariants. The Mooney–Rivlin model can be written in the form

$$W = \sum_{i,j=0}^{\infty} a_{ij}(I_1 - 3)^i(I_2 - 3)^j, \quad a_{00} = 0 \quad (1)$$

where I_1 and I_2 are the first and second strain invariants respectively and a_{ij} represents the model constants. As it is assumed that the material used in this study is soft and incompressible, $I_3 = 1$. It can be noted that I_3 is the same as J .

ANSYS 9.0 was used for the Mooney–Rivlin material model calculation. The nine coefficients are obtained by curve fitting the three recommended material characterization experiments. ANSYS allows the input of either the hyperelastic constants or the test data. When test data are used as the input, ANSYS calculates the hyperelastic constants and provides a quick graphical comparison of the material model response and the experimental data. The constants a_{ij} are determined by the true stress–strain curve obtained from the uniaxial tensile tests.

The least-squares error to be minimized during data fitting is based on absolute errors defined as

$$|R| = \sum_i (a'_i - a_i)^2 \quad (2)$$

where $|R|$ is the absolute error, a'_i is the measured datum, and a_i is the calculated datum. Equation (2) must be satisfied in order to ensure that the uniaxial data fit the obtained data. To calculate the absolute error a short custom code was applied.

2.4 Model constants

The material used for the artificial HV is PVA matrix reinforced by BC nanofibres; this is classified as an anisotropic short-fibre-reinforced nanocomposite.

The engineering values of the strain–stress curve of PVA–BC are curve fitted by the equation [19]

$$\sigma = y_0 + a e^{b\varepsilon} + c e^{d\varepsilon} \quad (3)$$

where σ is the engineering stress, ε is the non-uniform engineering strain, and y_0 , a , b , c , and d are fitting parameters (listed in Table 1). The elastic modulus as a function of strain was calculated as the first derivative of equation (3) with respect to strain.

For statistical comparisons, a two-way analysis of variance was performed, which is consistent with the statistical analysis performed previously [19, 20]. The engineering data are now transformed into the true strain–stress curve (Fig. 2) for both circumferential and longitudinal directions.

To determine the constants in equation (1) from the uniaxial tests, the stress–strain curve is converted to the strain energy density function by minimizing the absolute error presented in equation (2) using a non-linear regression analysis. The true stress–strain curves measured separately in the circumferential and longitudinal directions were curve fitted into three categories of the Mooney–Rivlin models with two, three, and five parameters. The constants of equation (1) for circumferential and longitudinal directions are given in Tables 2 and 3 respectively. These tables also outline the absolute errors with

Table 1 Model parameters of the mechanical properties of 15 wt% PVA–0.5 wt% BC

Coefficient	Longitudinal valve	Circumferential valve
a	0.037	0.031 62
b	1.335 99	4.781 97
c	0.001 96	0.032 06
d	8.031 96	6.517 87
y_0	–0.034 85	–0.058 55

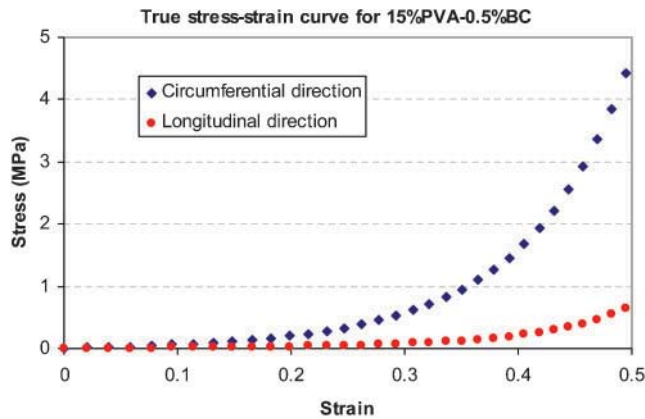


Fig. 2 The true strain–stress curve obtained from the experimental tensile test for the anisotropic 15 wt % PVA–0.5 wt % BC

each constitutive model when fitted to the experimental data. The parameter shown in Tables 2 and 3 describe the Mooney–Rivlin models, with various numbers of model constants.

2.5 Advance surfacing technique for the geometry of the HV

The free form of the HV leaflet refers to the curved line defining the free edge of the leaflet in contact with the two adjacent leaflets when viewed from the top. Revolution of this curve about the longitudinal axis of the aorta where each incremental rotation of the curve about the axis intersects the free edge forms the curve surface in both the longitudinal and the circumferential directions. Besides the leaflet geometry, other design parameters such as the thickness of the leaflet, which is not necessarily uniform, the diameter of the valve, the width of the posts of the stent, and the material properties of the leaflet and stent all have roles in the valve's mechanical behaviour.

In the literature, a special conicoid demonstrated poor leaflet opening characteristics and a high opening pressure gradient [22]. An ellipsoid of revolution has been demonstrated to have a restricted selection of the major axis and eccentricity of the ellipsoid as determined by the height of the valve [23]. A paraboloid of revolution with the focus at the base of valve was unacceptable because the radius of curvature of the leaflet is lower at the base of the leaflet, which inhibits valve opening [23]. A closed leaflet with an elliptical geometry in the radial direction and hyperbola in the circumferential direction has been reported to have regurgitation and leakage volume lower than both St. Jude bileaflet mechanical and St. Jude prosthetic valves with an equivalent valve size [24]. Leat and Fisher [23] reported a new geometry for the design of polyurethane leaflet HVs. The geometry termed the alphasphere has a radius of curvature that increases from the centre of the leaflet at the free edge towards the base of the valve and perimeter of the leaflet to improve the opening characteristics of the HV [22]. A more recent approach reported by Jiang *et al.* [22] used the revolution of the arc subtending two straight lines. Using this approach, PVA trileaflet valves with a smaller apex opening and reduced gap between adjacent leaflets were achieved [22]. The problems with the Jiang *et al.* model are, first, the gap between the two adjacent leaflets and, second, a relatively large orifice area in the centre of the HV which may compromise valve performance. Also, the use of hyperbolic function makes reaching the desired leaflet geometry impossible. More importantly, this design did not take into account the mechanical properties of the materials used.

In this section, a new design of a trileaflet HV based on the anisotropic PVA–BC material properties is described. This design addresses the problems related to the Jiang *et al.* design by, first, developing

Table 2 The hyperelastic parameters for the different types of Mooney–Rivlin model for the longitudinal direction

	a_{10}	a_{01}	a_{20}	a_{11}	a_{02}	Absolute error (%)
Two parameters	−0.144	−0.13	0	0	0	4.16
Three parameters	−0.446	0.499	0.0330	0	0	1.47
Five parameters	−3.906	4.095	27.240	−72.51	50.882	0.15

Table 3 The hyperelastic parameters for the different types of Mooney–Rivlin model for the circumferential direction

	a_{10}	a_{01}	a_{20}	a_{11}	a_{02}	Absolute error (%)
Two parameters	1.365	−1.374	0	0	0	3.38
Three parameters	2.790	3.053	2.396	0	0	0.98
Five parameters	−26.778	28.001	184.86	−492.57	346.379	0.07

a new approach to define valve leaflet geometry, second, minimizing the apex opening, and, third, incorporating the mechanical and material properties of the anisotropic PVA-BC material into the design process.

2.5.1 Bezier surface

The Bezier surface is formed as the Cartesian product of the blending functions of two orthogonal Bezier curves. A Bezier surface is a weighted sum of $n+1$ in the u direction and $m+1$ in the v direction of control points $P_{0,0}, \dots, P_{ij}$, where the weights are the polynomials [25]

$$f(x, y) = \underbrace{\sum_{i=1}^n \binom{n}{i} (1-x)^{n-i} x^i}_{\text{A}} \sum_{j=1}^m \binom{m}{j} (1-y)^{m-j} y^j P_{i,j} \rightarrow x, y \in [0, 1] \quad (4)$$

↑
B

Part A of this equation is called the blending function since it blends the control points to form the Bezier curve. This function is always a polynomial one degree less than the number of the control points. Part B is the control points in the u and v directions. A Bezier surface is chosen in this study since Bezier surfaces do not pass through any of the control points except those located at the boundaries. One important advantage of Bezier surfaces is that the surface is always contained within the convex framework of the control points and it never oscillates widely away from the control points. To design the leaflet geometry, first the boundaries of the HV leaflet, which consist of the commissure and the free edges, are designed and then a limited number of control points are used to produce the desired Bezier surface.

There are two ways to describe the fully closed form of the HV leaflet to obtain the necessary control points to create the geometry: first, by mapping the leaflet geometry of a trileaflet bioprosthetic valve,

which can be achieved using a coordinate measuring machine with a laser scanning system (e.g. 3D Digital Corp, three-dimensional (3D) scanner cyberware) or other digitizing systems [22], and, second, by deriving the necessary control points from the equations used in the Jiang *et al.* [22] model. The second option is chosen as the equations for the leaflet geometry are already available to us. As the number of control points increases, it is necessary to have higher-order polynomials and possibly factorials. Hence, an efficient algorithm for this conversion is highly desired. Degree reduction of a Bezier surface is a process in which one Bezier polynomial is approximated by another of lower degree. The

process of degree reduction is carried out by minimizing the L2 norm between the two surfaces (the Jiang *et al.* model and the current model). The degree reduction of Bezier surfaces is considered as solving the inconsistent linear system using the least-squares method demonstrated in Fig. 3. Figure 4 shows the order reduction of the concave shape of the leaflet geometry as a Bezier-type surface by changing the number of control points in an evaluation process. The six Bezier subsurfaces constructed to create the HV leaflet geometry using 50 control points are shown in Fig. 4. The first version of this model is produced in computer aided design (CAD) software, Mechanical Desktop 2006, using the six Bezier subsurfaces assembled in Fig. 5(a). The number of vertices in this wireframe is 51 (Fig. 5(b)) including 22 boundary vertices which consist of nine vertices on the free edge and 15 on the commissure edge, with 29 central control points optimally distributed all over the surface of the leaflet. The first derivative is matched as the tangent at the boundaries of the subsurfaces at the end of one

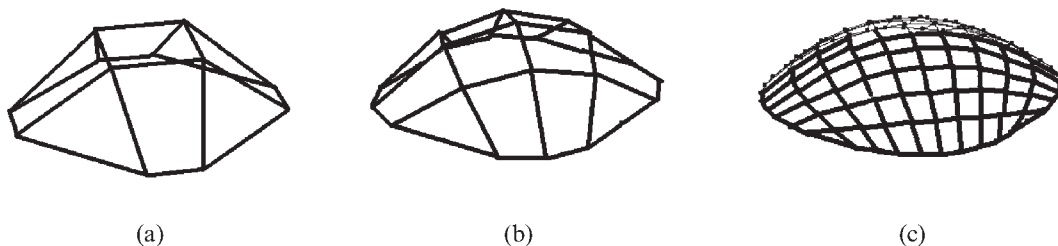


Fig. 3 Developing the leaflet geometry using a 3×3 tensor product: (a) degree evaluation ($r = 1$); (b) degree of evaluation ($r = 2$); (c) repeated degree evaluation r

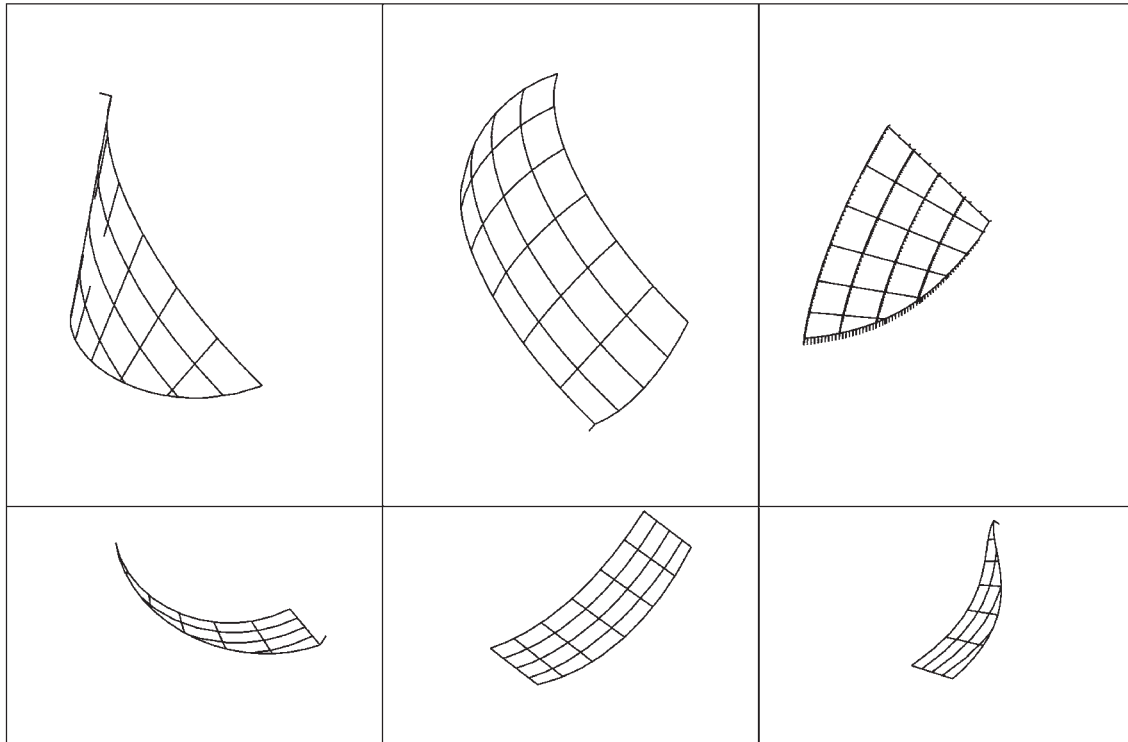


Fig. 4 The Bezier subsurfaces for the construction of the leaflet geometry

piece must be along the next piece (C_1) but second-order continuity (C_2) is not necessary.

2.5.2 The final model

To form the final model, starting with the geometry of the leaflet, the free and commissure edges can be tailored as desired. One of the advantages of this approach is the elimination of gap between the two adjacent leaflets in the first stage of the design of the final geometry of the valve leaflets. Also, the free-edge design is based on the use of the biomaterial, i.e. PVA-

BC. This is applicable by applying the FE model to ensure that the orifice area is reasonably small when the valve is fully closed (end of diastole). By manipulating the control points on the free edge and analysing the new geometry with the FE procedure shown in Fig. 6, it is ensured that the orifice area at the centre of the valve is sufficiently small when it is fully closed. Finally, a CAD model of free-form leaflet geometry using a Bezier-type surface is designed, which is shown in Fig. 7. The stent dimensions were replicated from the Medtronic Mosaic aortic bioprosthesis model 305 [26]. The dimensions used for the stent are given in Table 4.

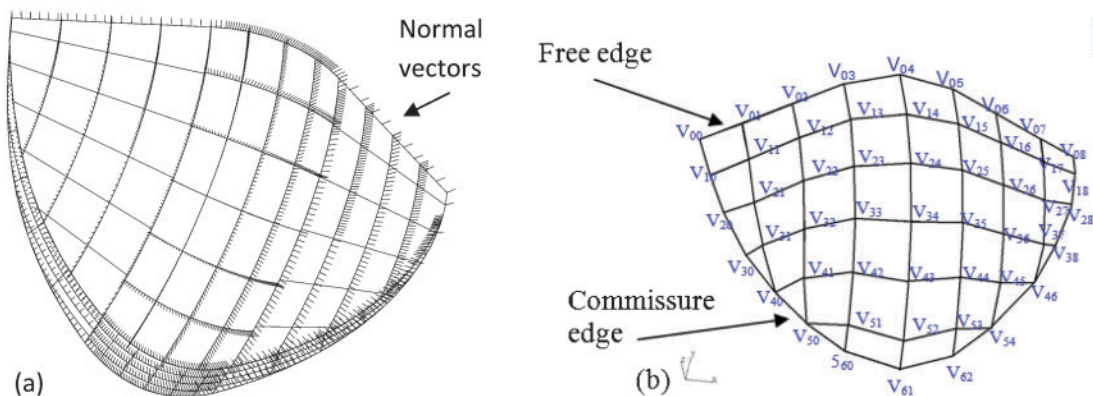


Fig. 5 (a) The assembled Bezier patches concerning the surface parameters, e.g. the tangent plane, normal vectors as illustrated in the figure; (b) the final wire frame model

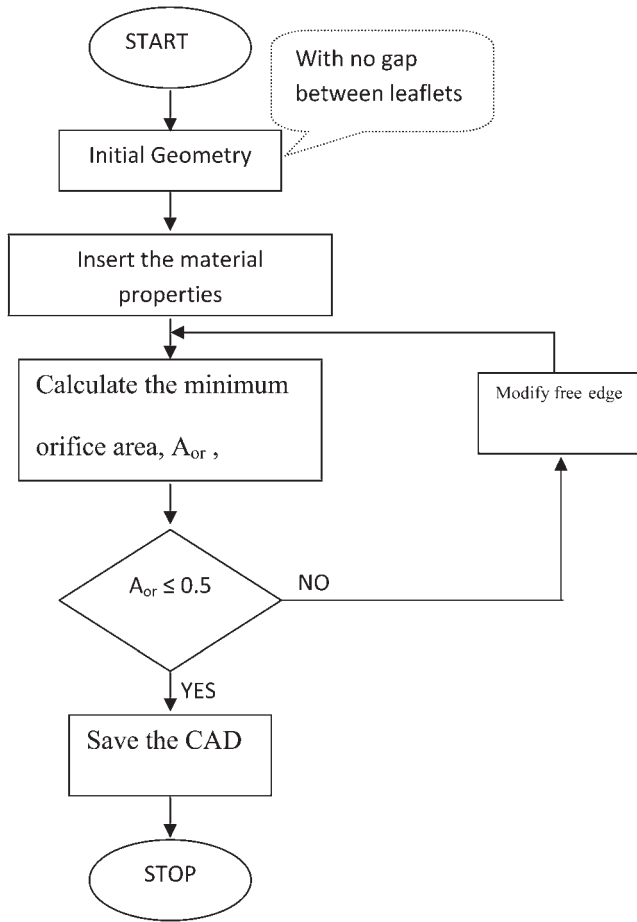


Fig. 6 Flow chart scheme to correct the leaflet geometry in an iteration process. A_{or} is compared with the total opening area and is set to zero when the ratio of A_{or} to the total area is less than 5 per cent

In order to improve the surface quality, as the final refinement of the surface, Bezier curves were adjusted through a trial-and-error process by relocating, removing, or interpolating the control

Table 4 Dimensions of the heart valve stent

Valve size (outer diameter of the stent)	30.0 mm
Orifice diameter (inner diameter of the stent)	28.0 mm
Sewing ring diameter	35.0 mm
Valve height	17.5 mm
Aortic protrusion (valve height minus the height of the saddle arc on the sewing ring)	14.5 mm

points. The present 3D CAD model was then created by using a command to be converted to a shell in any available CAD software, e.g. command Shell of I-Deas in which a uniform thickness is required to produce a shell through the designed Bezier surface. We used Mechanical Desktop V2005i CAD software to produce the surfaces. The final model consists of three identical leaflets, with each leaflet being symmetrical about its own midline between the top of the free edge to the midpoint of the commissure of the leaflet shown in Fig. 7. In this section, an advance surfacing technique is introduced for complicated geometries such as HV leaflets that are more refined compared with the former designs as it is reproducible, computationally fast, easy to manipulate, and easy to combine with other segments or other surfaces. This approach when used in combination with material properties and a finite element method (FEM) solution can provide an optimum design of mechanical HVs and other medical devices and this is the approach that was taken.

2.6 The finite element model

2.6.1 FEM software and anisotropy

Mechanical modelling of soft tissues using hyper-elastic anisotropic elements is not available directly in any FE commercial software. The material model used in the anisotropic PVA-BC nanocomposite,

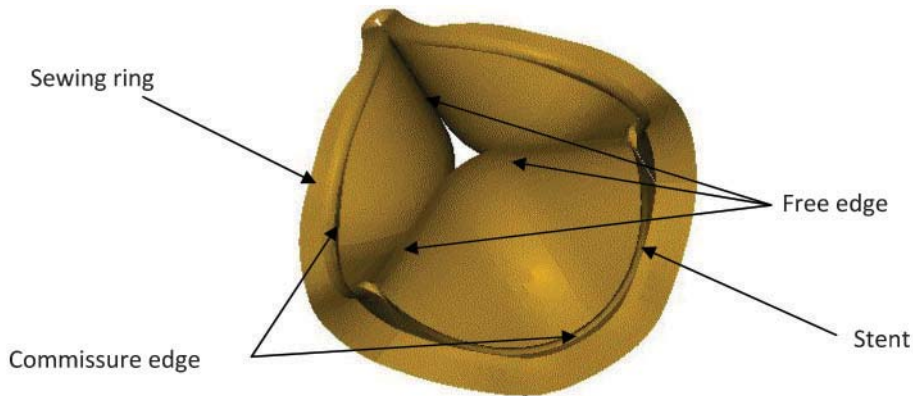


Fig. 7 The final geometry of the PVA-BC heart valve. The gaps between the two adjacent leaflets have been eliminated and the orifice area in the middle of the valve will be less than 5 per cent of the total orifice area of the valve in the fully closed position

consisting of an isotropic PVA matrix reinforced with BC homogeneously embedded in the circumferential direction similar to the distribution of collagen fibres in the aortic HV leaflet. The principal axes are defined in directions parallel and perpendicular to the BC fibres. In the material model, the fibres are assumed to behave like ropes since they cannot withstand a bending moment. Available elements that possess such properties in commercial FE software are spar elements. The PVA matrix is described by the Mooney–Rivlin model for isotropic hyperelastic material. This can be solved using the commercial FE software package ANSYS. In the FE mesh the diameter of individual spar elements for each PVA matrix is calculated as the BC volume fraction in a composite Voigt model (Fig. 8).

2.6.2 Boundary conditions

(a) Leaflet contact. The contact surfaces and the corresponding force are determined by interactive

computation of a pushback force which is calculated on nodes. To characterize the kinematics of the contact, two symmetrical leaflets are defined whose surfaces are ∂s_1 and ∂s_2 in 3D space, as shown in Fig. 9. The distance from each point on the leaflet from the central plane is defined by a scalar function $g(x)$, which is the ‘gap’ function. Assuming frictionless contact, the contact force must be normal to the surface of the leaflets. The normal vector is a partial derivative of $g(x)$ with respect to the spatial coordinates. Thus, the contact force is [27]

$$F_n = \frac{\partial g(x)}{\partial x} = F \nabla g \tag{5}$$

The penalty method replaces the contact force with the penalty $\epsilon_F g$, as shown in Fig. 10. As in the FEM, all forces must be discretized into a nodal equivalent force; the contact force in the penalty formulation is discretized as [27]

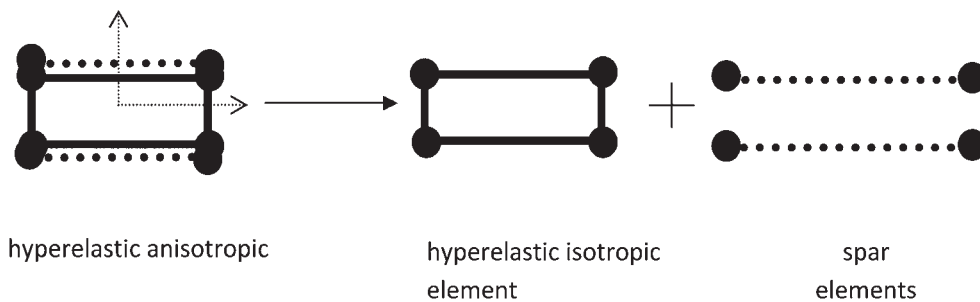


Fig. 8 Anisotropy through a hybrid element, a combination of an isotropic hyperelastic element, and a spar element oriented in the circumferential direction

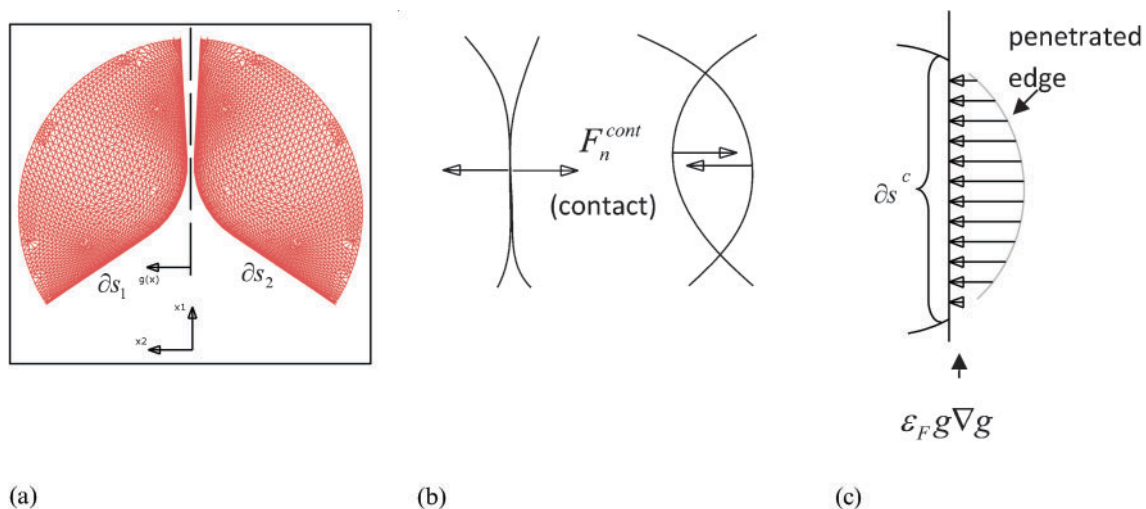


Fig. 9 (a) geometry of the leaflets to be solved for a pushback contact solution; (b) surfaces before and after contact; (c) penalty method to contact force

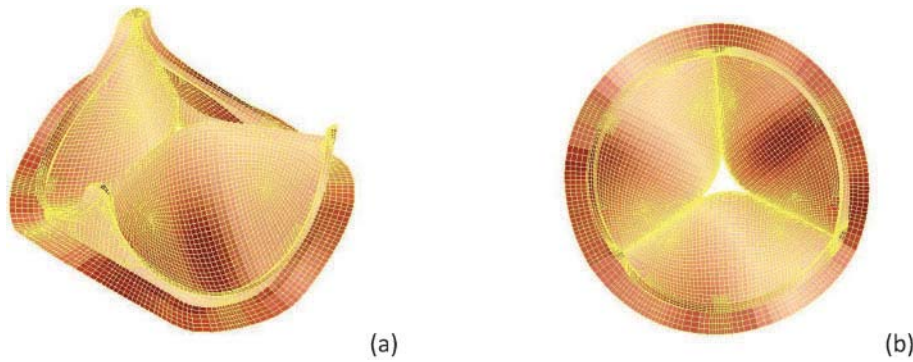


Fig. 10 The FE model of the PVA-BC heart valve in (a) an isometric view and (b) a top view including the leaflets, stent, and sewing ring

$$F_e^{cont} = \int_{\partial s^c} \varepsilon_{FG} \nabla g N_e(x_1, x_2) da \quad (6)$$

where $\varepsilon_{FG} \nabla g$ is the contact penalty force, N_e is the shape function, ∂s^c is the contact area, da is the element area, and F_e^{cont} is the nodal equivalent contact force on node e .

(b) *Load and displacement boundary conditions.* The leaflets are assumed to be located in a cylindrical conduit with material properties of the aortic root. The aortic side of the HV is assumed to be under a uniform systolic pressure of 120 mmHg. The pressure increment is $\Delta p_n = \frac{P^*}{N}$, where P^* is the maximum systolic pressure and N is the number of increments.

(c) *Finite element model specifications.* The geometry is covered with eight-node quadrilateral non-linear hyperelastic 3D shell elements reinforced with 3D non-linear spar elements uniformly distributed in the circumferential direction. Grid independence checks show a node number of 14 904 and an element number of 10 798 are sufficient for the present model. The element properties and the FE model used in this study are listed in Table 5 and Fig. 10 respectively.

Table 5 Specifications of the elements for the BC-PVA heart valve with the criteria for an aspect ratio less than 5, a warp angle less than 7, a skew angle (for 95 per cent of elements) less than 30, and a taper (for 95 per cent of elements) greater than 0.8

Test	Worst case (total failed)	Location
Aspect	Maximum, 4.141(0)	Stent
Warp	Maximum, 9.151(2)	Stent
Skew	Maximum, 62.373(324)	Stent
Taper	Minimum, 0.542(326)	Stent

3 RESULTS

The mechanical response of porcine HV in both principal directions were compared against the anisotropic 15 wt% PVA-0.5 wt% BC samples (Fig. 11), which was one of the stiffest materials for a possible match of the tensile properties for the tissue replacement applications [28]. Although a close match was not obtained for HV tissues previously, both principal directions of the anisotropic PVA-BC sample (75 per cent initial strain and cycle 4) fall within the circumferential and radial curves, around the physiological range, as seen in Fig. 12. This hydrogel displays higher tensile stress than HV at low strains (less than 20 per cent), with

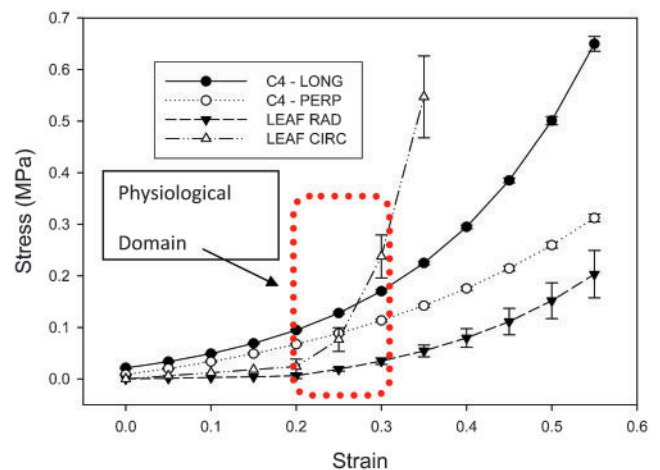


Fig. 11 Comparison of anisotropy of porcine heart valve (both directions) and 15 wt% PVA-0.5 wt% BC nanocomposite with 75 per cent initial strain (cycle 4). Longitudinal and perpendicular directions in the PVA-BC nanocomposite correspond to the circumferential and radial directions in the porcine leaflet tissue respectively. The physiological range of strain is between 20 per cent and 30 per cent

the circumferential HV samples drastically increasing their modulus at larger strains (greater than 20 per cent), surpassing that of any PVA–BC hydrogel tested. This high-stiffness anisotropic PVA–BC nanocomposite would be a better match for the anisotropic behaviour of HV than any isotropic biomaterials.

Based on the geometry and the FE model developed, calculations were performed to assess the distribution and magnitude of mechanical stresses and bending moment on the HV leaflet. In addition, valve dynamics were examined as a function of the cardiac cycle.

3.1 Valve thickness

The thickness of the heart valve leaflet is not uniform and varies over a range from 0.1 mm to 1.4 mm [15]. In the current design, it is assumed that the leaflets are of uniform thickness. The criteria used to determine the thickness of the leaflet are based on the critical values of principal stresses and bending moments reported for the porcine aortic heart valve by Li *et al.* [15]. Using those criteria, it was found that the thickness of 0.7 mm provides the closest match by performing a parametric study on the leaflet with a thickness starting from 0.1 mm to 1.1 mm.

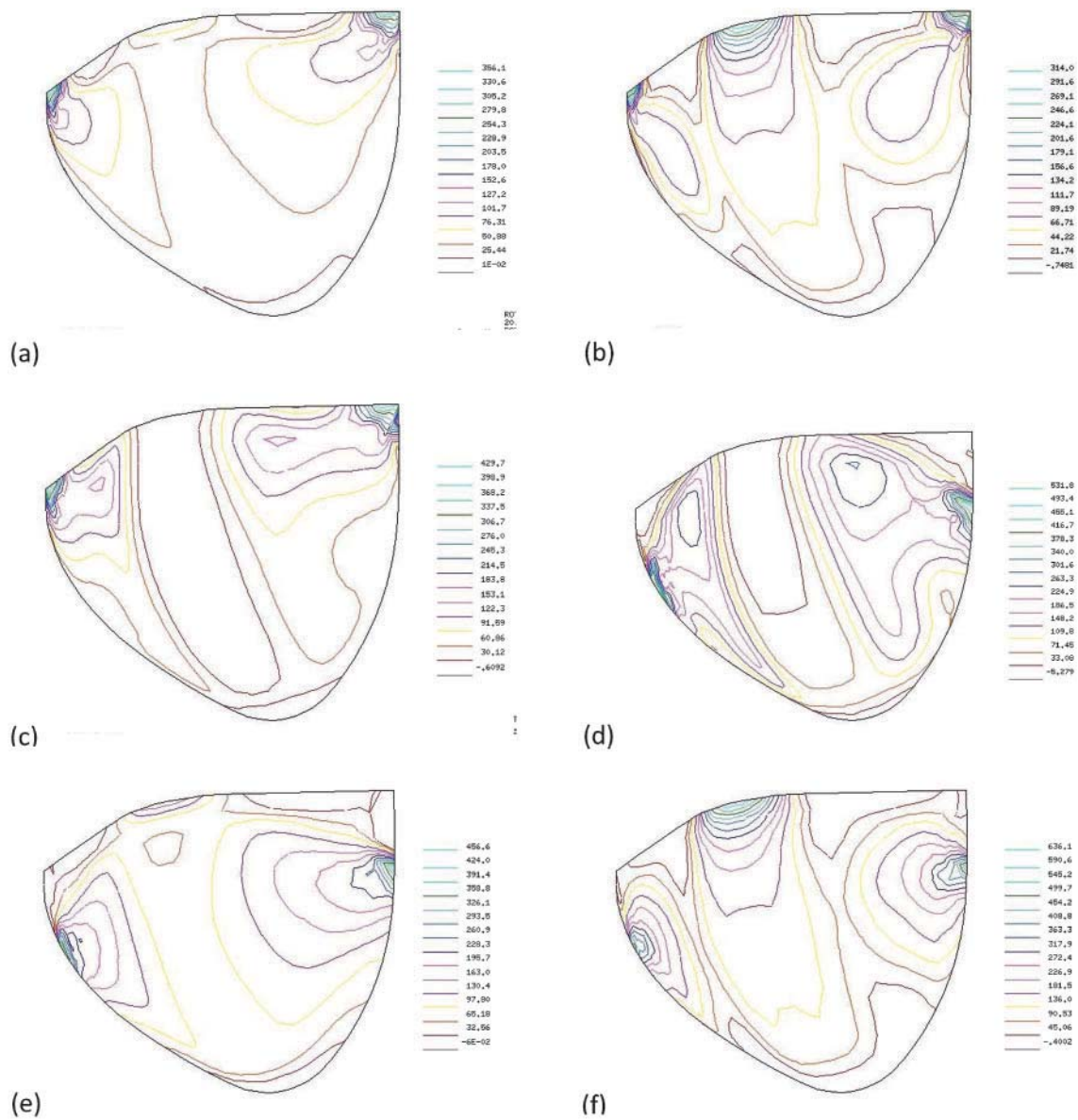


Fig. 12 Stress distribution (the first principal stresses) for (a)–(c) isotropic and (d)–(f) anisotropic in a layered structure for the leaflets: (a), (d) the middle layer; (b), (e) the top layer; (c), (f) the bottom layer. Values in the spectrum are given in kilopascals

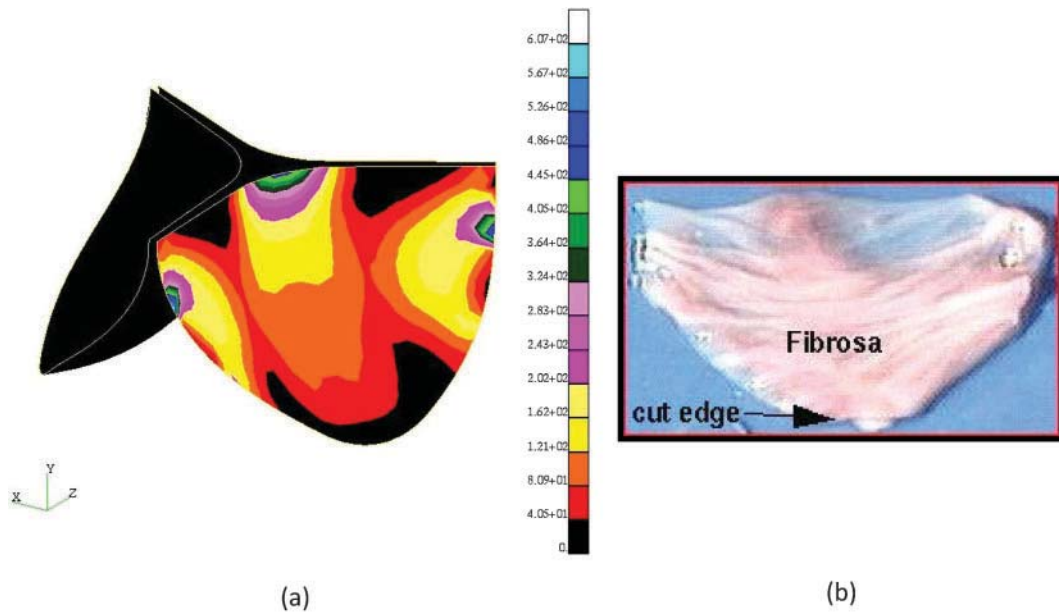


Fig. 13 The correspondence between (a) the maximum or minimum principal stress and (b) the highest or lowest collagen fibre content [29]. The values in the colour bar are in kilopascals

3.2 Distribution of principal stresses on the leaflet

The stress distribution and maximum principal stresses on leaflets are shown in Fig. 12 for the isotropic and anisotropic models. In the isotropic model, the maximum principal stress is located at the corners of the leaflets where free and commissure edges intersect. If the leaflet is assumed to be a layer structure including top, middle, and bottom layers as is the case for aortic HV leaflet tissue, the maximum principal stresses in these layers for the isotropic model will be 314 kPa, 356 kPa, and 429 kPa (Figs 12(a), (b), and (c) respectively).

In the anisotropic model, locations of high stress zones and the maximum stress values are significantly different (Figs 12(d), (e), and (f)). The maximum principal stresses are 636 kPa, 486 kPa, and 531 kPa in a layered structure. It can be seen that, although the maximum principal stresses for the layered structure are similar in both models, there are significant differences in the locations of these stress distributions on the HV leaflets composed of PVA-BC nanocomposite. Li *et al.* [15] reported similar locations and values for high-stress regions in porcine HV leaflets using an anisotropic model. These results further re-

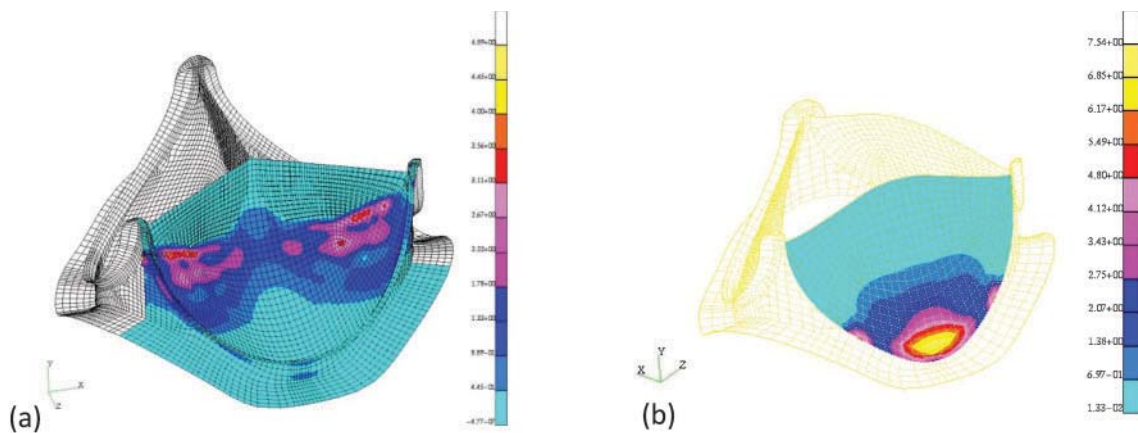


Fig. 14 The distribution of the tensile bending moment per unit length on leaflets (a) when the valve is fully closed and (b) when the valve is widely open. The values are given in millinewtons

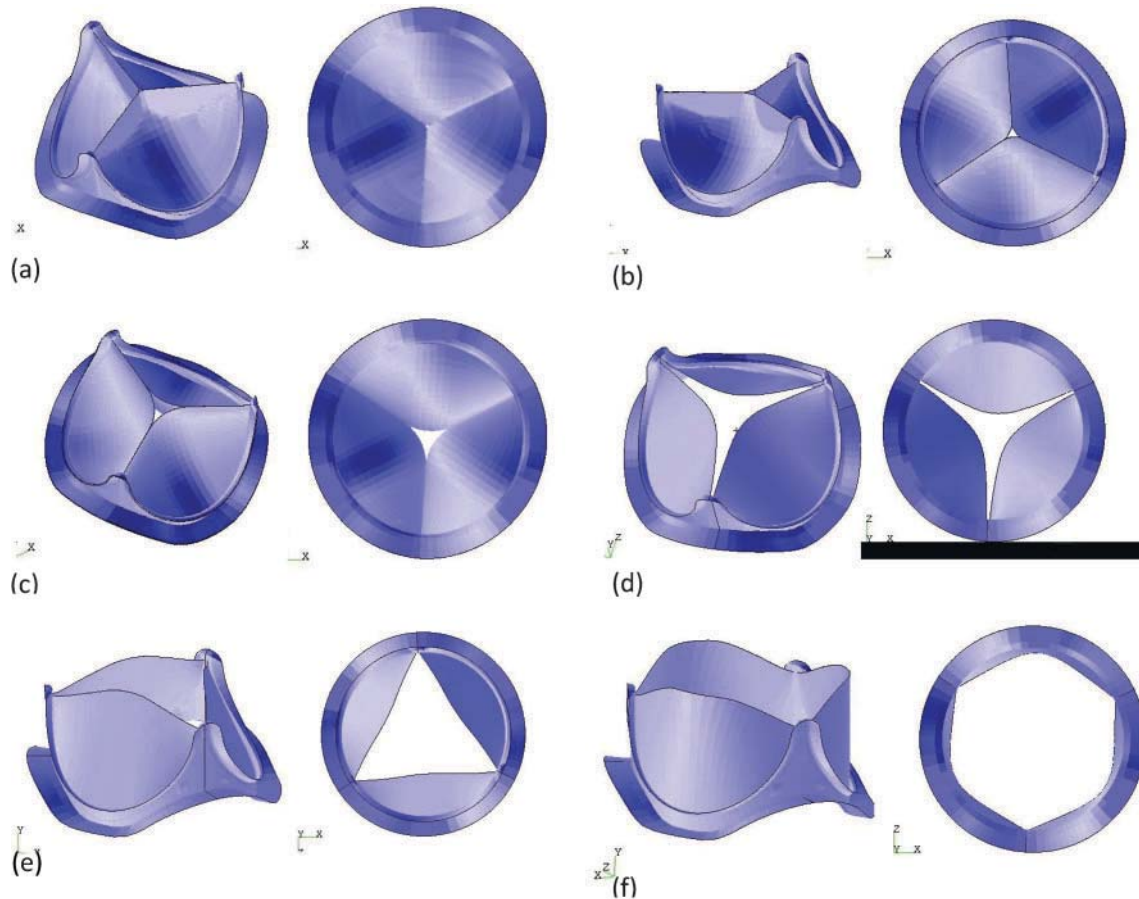


Fig. 15 The valve motion during the closing and opening phases: (a) when the valve is fully closed and the contact area has its maximum value; (b) when the contact area is still developing and the small orifice area in the middle of the valve is becoming smaller owing to the deformation of the leaflets; (c) the initial situation; (d)–(f) the opening phase when the structure of the leaflets becomes geometrically unstable

inforce the validities of the present anisotropic FE model.

As the first attempt in the study of mechanical behaviour of HVs under physiological conditions, also the results of the locations of the high-stress zones in the present anisotropic model and the organization of collagen fibres in terms of their distribution and concentration in the porcine HV leaflet were compared. Since collagens are a load-bearing matrix protein, its fibres are used to strengthen the leaflet structure. It would be expected that regions that experience high stresses would be reinforced with high concentration of collagen fibres. As seen in Fig. 13, there is a close correspondence between the high–low-stress zone simulated in our model shown in Fig. 13 and the distribution of collagen fibres in the porcine aortic HV leaflet. In contrast with the anisotropic model, the result for the isotropic model shown in Figs 12(a), (b), and (c) indicate that the maximum principal stress

regions do not correspond to the regions of high collagen fibre densities (Fig. 13(b)).

3.3 Bending moment

In the anisotropic model, the effective bending moment per unit length is computed from the Cauchy stress tensor in the top and bottom layers of the leaflets in the opening (Fig. 14(a)) and closing (Fig. 14(b)) phases. For the closing phase, the crucial zone is located under contact areas with the maximum value of 4.89 mN mm/mm. In the opening phase, the maximum bending moment is 7.54 mN mm/mm located close to the commissure edge on the midline. The distributions of the bending moment calculated for the closing phase are in agreement with those of the Li *et al.* [15] model (less than 8 per cent error). It is also consistent with collagen fibre distributions in an aortic HV leaflet shown in Fig. 13(b).

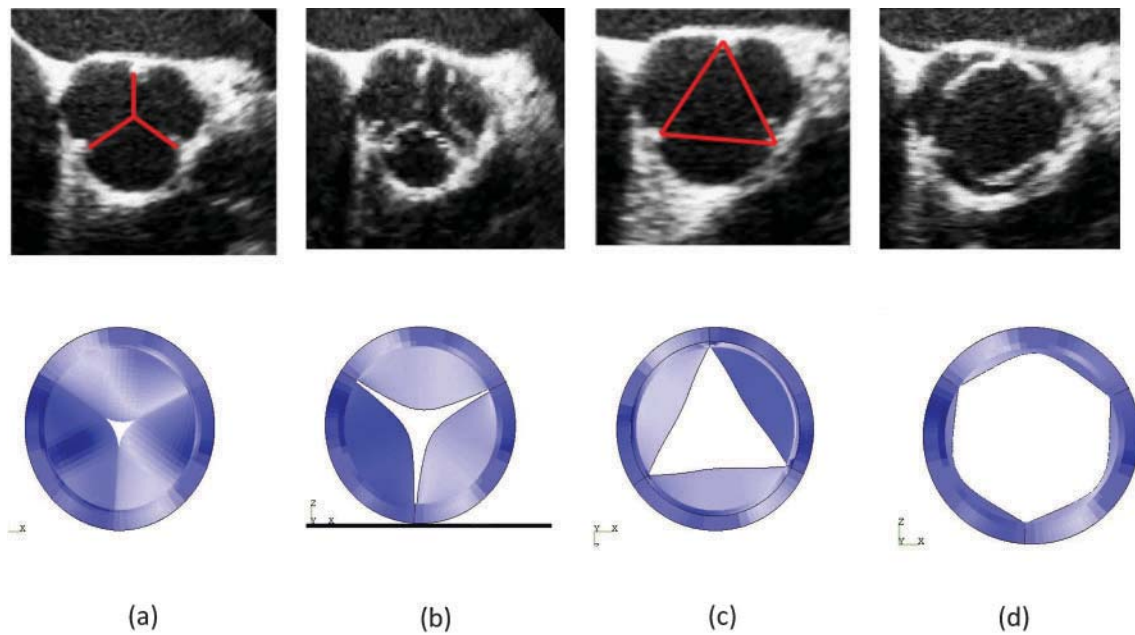


Fig. 16 The comparison of the FEM results and the ultrasound images in support of the simulation in the opening phase: (a) the initial state of opening phase; (b) the boomerang shape of the free edges at the beginning of the opening phase; (c) the triangular shape of the free edges; (d) the hexagonal shape of the free edges which closely match the ultrasound images

3.4 Valve dynamics

Figure 15 indicates the dynamic valve motion during systole and diastole in the anisotropic PVA-BC model. The contact area, the deformation of HV, and the geometry of the leaflets were simulated in the opening and closing phases. Figure 15(a) is when the valve is fully closed and the contact area is at its maximum value. Figure 15(b) is when the contact area is still developing and the small orifice area in the middle of the valve becomes closed owing to deformation of the leaflets. Figure 15(c) indicates the initial state of the cardiac cycle. Figures 15(d), (e), and (f) show the progressive stages of the opening phase when the leaflets undergo large displacement and become geometrically unstable, e.g. buckling. Simulation of the stages in the opening phase has also been validated with the ultrasound images of the aortic HV. The initial state of the valve when the HV leaflets start to open is shown in Fig. 16(a). The formation of a boomerang shape of the free edges in the beginning of the opening phase is shown in Fig. 16(b). The formation of the triangular shape and the hexagonal shape of free edges are also shown in Figs 16(c) and (d) respectively.

The FE model developed on the basis of the anisotropic PVA-BC material simulates the proper distribution and location of principal stresses and bending moments that correspond well to the collagen fibres distribution in the porcine aortic

valve leaflet tissue. Moreover, it also predicts the close performance of an anisotropic PVA-BC-based trileaflet mechanical aortic valve to that of the native aortic HV. This model would be valuable for the design of trileaflet mechanical HVs based on hyperelastic and anisotropic material.

4 CONCLUSION

A trileaflet mechanical HV based on the PVA-BC nanocomposite material has been designed. A new hybrid element which is a combination of hyperelastic non-linear isotropic elements and 3D membrane spar elements has been developed to analyse a trileaflet PVA-BC nanocomposite mechanical HV prosthesis mechanically. The new PVA-BC nanocomposite material was designed to possess similar mechanical properties to the porcine HV leaflet. The stress pattern, maximum principal stresses, Cauchy stress tensor, and distribution of bending moments in the closing and opening phases have been calculated. Contact between the adjacent leaflets, the orifice area located in the middle of the valve at each step, the geometrical instability in the opening phase, and the minimum thickness of the leaflets for the PVA-BC mechanical HV were computed for use in improving the design of mechanical HVs.

The results indicate a significant difference between the mechanical behaviours of the isotropic and the anisotropic models. The anisotropic model is consistent with the actual porcine aortic HV and accurately predicts the distribution of collagen fibres in the HV leaflet tissue. Li *et al.* [15] reported that the maximum bending moment is located under the contact area in the closing phase and Burriesci *et al.* [14] reported that the high bending moment area is near the commissure edge in the opening phase. These data in the literature further validate the present results.

In the design and modelling of the anisotropic PVA-BC nanocomposite-based trileaflet mechanical HV, the material parameters input was limited to two, namely the elastic moduli of the composite in two orthogonal directions. This limitation arose because only uniaxial tensile testing was performed, as a biaxial testing facility is not available in the present authors' laboratory. Improvements can be made by obtaining a full set of the necessary material properties parameters including the shear modulus and Poisson's ratios. However, biaxial testing on the composite material will be required. Future work should consider the acquisition of these parameters as they are relevant not only to mechanical HV design but also to other soft tissue-related devices and in tissue engineering.

ACKNOWLEDGEMENTS

The authors thank the Integrated Manufacturing Technology Institute and the Virtual Environment Technology Centre for providing technical supports and facilities to achieve this project. The authors also thank the Canadian Institutes of Health Research for funding this project.

REFERENCES

- Mackay, T. G., Wheatley, D. J., Bernacca, G. M., Fisher, A. C., and Hindle, C. S. New polyurethane heart valve prosthesis: design, manufacture and evaluation. *Biomaterials*, 1996, **17**, 1857–1863.
- Nistal, F., Garcia-Martinez, V., Arbe, E., Fernandez, D., Artinano, E., Mazorra, F., and Gallo, I. *In vivo* experimental assessment of polytetrafluoroethylene trileaflet heart valve prosthesis. *J. Thoracic Cardiovascular Surg.*, 1990, **99**, 1047–1081.
- Knierbin, B., Rosarius, N., Unger, A., Reul, H., and Rau, G. CAD design, stress analysis and *in vitro* evaluation of three leaflet blood-pump valves. *J. Biomed. Engng*, 1992, **14**, 275–286.
- Wijsmuller, E. G., Yu, L. S., Yuan, B., Bishop, N. D., and Kolff, W. J. Development of a new inflow valve for a 20 cc semisoft ventricle: preliminary results. *Int. J. Artif. Organs*, 1990, **13**, 503–508.
- Mohammadi, H., Klassen, R. J., and Wan, W. K. A finite element model on effects of impact load and cavitation on fatigue crack propagation in mechanical bileaflet aortic heart valve. *Proc. IMechE, Part H: J. Engineering in Medicine*, 2008, **222**(7), 1115–1125. DOI: 10.1243/09544119JEIM432.
- Gould, P. L., Cataloglu, A., Dhatt, G., Chattopadhyay, A., and Clark, R. Stress analysis of the human aortic valve, computers and structures. *Comput. Structs*, 1973, **3**, 377–384.
- Krucinski, S., Vesely, I., and Dokanish, M. A. Numerical simulation of leaflet flexure in bioprosthetic valve mounted on rigid and expandable sterns. *J. Biomech.*, 1993, **26**, 929–943.
- Patterson, E. A., Howard, I. C., and Thornton, M. A. A comparative study of linear and nonlinear simulations of the leaflets in a bioprosthetic heart valve during the cardiac cycle. *J. Med. Engng Technol.*, 1996, **20**, 95–108.
- Grande, K. J., Cochran, R. P., and Reinhall, P. G. Finite element analysis of aortic heart valve sparing: influence of graft shape and stiffness. *IEEE Trans. Biomed. Engng*, 2001, **48**, 647–654.
- Beck, A., Thubrikar, M. J., and Robicsek, F. Stress analysis of the aortic valve with and without sinuses of valvular. *J. Heart Valve Dis.*, 2001, **10**, 1–11.
- Mohammadi, H., Ahmadian, M. T., and Wan, W. K. Time-dependent analysis of leaflets in mechanical aortic bileaflet valve in closing phase using the finite strip method. *J. Med. Engng Phys.*, 2006, **28**, 122–133.
- Rousseau, E. P. M., Sauren, A. A. H. J., and Hout, M. C. V. Elastic and viscoplastic material behaviour of fresh and glutaraldehyde-treated porcine aortic valve tissue. *J. Biomech.*, 1983, **16**, 339–348.
- Sripathi, V. C., Kumar, R. K., and Balakrishnam, K. R. Further insights into normal aortic heart valve functions; rule of compliant aortic root on leaflet opening and valve orifice area. *Ann. Thoracic Surg.*, 2004, **77**, 844–851.
- Burriesci, G., Haward, I. C., and Patterson, E. A. The stress/strain and fatigue behaviour of glutaraldehyde preserved heart valve tissue. *J. Biomech.*, 1999, **10**, 707–724.
- Li, J., Lou, X. Y., and Kuang, Z. B. A nonlinear anisotropic model for porcine heart valves. *J. Biomech.*, 2001, **34**, 1279–1289.
- Luo, X. Y., Li, W. G., and Li, J. Geometrical stress reduction factors in anisotropic porcine heart valves. *Trans. ASME, J. Biomech. Engng*, 2003, **125**, 735–744.
- De Hart, J., Peters, G. W. M., Schreurs, P. G. J., and Baaijens, F. P. T. Collagen fibers reduce stresses and stabilize motion of aortic valve leaflets during systole. *J. Biomech.*, 2004, **37**, 303–311.
- Kim, H., Jia, L., Sacks, M. S., and Chandran, C. B. Dynamic simulation precordial bioprosthetic valve

- function. *Trans. ASME, J. Biomech. Engng*, 2006, **128**, 717–727.
- 19 **Millon, L. E., Mohammadi, H., and Wan, W. K.** Anisotropic polyvinyl alcohol for cardiovascular applications. *J. Biomed. Mater. Res. B; Appl. Biomater.*, 2006, **79**, 305–311.
- 20 **Millon, L. E. and Wan, W. K.** The polyvinyl alcohol – bacterial cellulose as a new nanocomposite for biomedical applications. *J. Biomed. Mater. Res. B; Appl. Biomater.*, 2006, **79**, 245–253.
- 21 **Guhados, G., Wan, W. K., and Hutter, J.** Measurement of the elastic modulus of single bacterial cellulose fibers using atomic force microscopy. *Langmuir*, 2005, **21**, 6642–6646.
- 22 **Jiang, H., Campbell, G., Boughner, D., Wan, W. K., and Quantz, M.** Design and manufacturing of polyvinyl alcohol cryogel tri-leaflet heart valve prosthesis. *J. Med. Engng Phys.*, 2003, **24**, 267–277.
- 23 **Leat, M. E. and Fisher, J.** A synthetic leaflet heart valve with improved opening characteristics. *Med. Engng Phys.*, 1994, **16**, 470–476.
- 24 **Mercer, J. I., Benedicty, M., and Bahnson, H. T.** The geometry and construction of the aortic leaflet. *J. Thoracic Cardiovascular Surg.*, 1973, **65**, 511–518.
- 25 **Gerald, F.** *Curves and surfaces for computer aided geometric design: a practical guide*, 1993 (Academic Press, New York).
- 26 **Yoganathan, A. P., Eberhardt, C., and Walker, P. G.** Hydrodynamic performance of the Medtronic Freestyle aortic root bioprosthesis. *J. Heart Valve Dis.*, 1994, **3**, 571–580.
- 27 **Keiser, R., Müller, M., Heidelberger, B., Teschner, M., and Gross, M.** Contact handling for deformable point-based objects. In *Proceedings of Vision, Modelling, Visualization (VMV'04)*, Stanford, USA, 2004, pp. 315–322.
- 28 **He, Z., Xi, B., Zhu, K., and Hwang, N. H. C.** Mechanisms of mechanical heart valve cavitation: investigation using a tilting disk valve model. *J. Heart Valve Dis.*, 2001, **10**, 666–674.
- 29 The Heart Valve Lab, The University of Western Ontario, What does a real heart look like? Dissecting a porcine (pig) heart (continued), 1997, available from <http://heartlab.robarts.ca/dissect/dissection2.html>.